Supplementary information for

“Surface Plasmon-Polariton Triggering of $Ti_3C_2T_x$ MXene Catalytic Activity for Hydrogen Evolution Reaction Enhancement”

A. Zabelina[a], D. Zabelin[a], E. Miliutina[a], J. Lancok[b], V. Svorcik[a], S. Chertopalov[b], O. Lyutakov

[a] *Department of Solid State Engineering, University of Chemistry and Technology, 16628 Prague, Czech Republic*
[b] *Institute of Physics of the Czech Academy of Sciences, Na Slovance 1999/2, 18221, Prague, Czech Republic*

Experimental part

Materials

Solution of Su-8 was purchased from Microchem, Germany, Au target for metal deposition (purity of metal 4 N) was provided by Safina, potassium carbonate and deionized water were purchased from Sigma-Aldrich. All chemical reagents were used as received without further purification. Ti powder (99 % metal basis, #325 mesh), Al powder (99.5 % metal basis, #325 mesh), and graphite (99 %, APS 7-11 micron) were purchased from Alfa Aesar.

Sample’s preparation

Au grating preparation. Su-8 films were spin-coated from a solution onto cleaned by acetone glass substrates. The prepared samples were dried and irradiated by UV lamp. After that, the polymer surface was patterned by KrF excimer laser (COMPexPro 50F, Coherent, Inc., wavelength 248 nm, pulse duration 20-40 ns, repetition rate 10 Hz), according to [S1]. Then 25 nm thick gold films were deposited onto the patterned surface by vacuum sputtering (DC Ar plasma, Ar gas purity of 99.995 %, gas pressure of 4 Pa, discharge power of 7.5 W, sputtering time 400 s).

Preparation of Ti_3AlC_2 MAX phase. The synthesis of the Ti_3AlC_2 MAX phase was performed by the procedure described in [S2]. The Ti, Al, and graphite powders in a 3.00:1.10:1.88 molar ratio were mixed with zirconia balls (diameter 3 mm) by ball milling at 60 rpm during 3 hours in a plastic jar. The mixed powders were putted into an Al boat and transferred to a tube furnace (4016T, Clasic CZ). Before synthesis, vacuum pumping was carried out twice with a pressure of 2 mbar, followed by a purge with argon. The MAX phase synthesis was accomplished by heating the mixture at 10°C/min to 1550°C in argon atmosphere followed by 2 hours holding period at 1550°C and cooling down to room temperature at 10°C/min.

Preparation of $Ti_3C_2T_x$* MXene *flakes. The $Ti_3C_2T_x$ MXene was synthesized using the MILD method described in [S2]. Before selective etching of aluminum from Ti_3AlC_2 MAX phase, the MAX phase ceramics were crushed by mortar and pestle and sieved to separate the particles of size below 45 μm. The etchant was prepared by dissolving 300 mg of LiF in 6 mL of 6 M HCl in a plastic centrifuge tube with a stirrer. Then, 300 mg of sieved MAX phase powder (particle size below 45 μm) was added to the prepared etchant and stirred at 22°C for 24 hours. After etching, the MXene were washed several times until the pH of the supernatant reached 5.5. Delamination of MXene flakes was carried out by hand shaking of the sample (15 mL DI water in a 50 mL plastic test tube) for 5 min followed by 30 min of centrifugation at 3500 rpm to precipitate and separate the non-delaminated MXene.

***MXene flakes shredding**.* The MXene flakes were separated from water by centrifugation and redispersed in N_2-saturated DMSO (3 mg/mL) in oxygen-free conditions. Then, the additional application of high power ultrasound (200 W, suspension volume – 20 mL, 30 min.) was applied for flakes shredding and formation of smaller flakes. The experimental procedure was optimized with the aim to avoid flakes oxidation or excessive degradation, and as optimal route the application of high-power ultrasound treatment during 15 min. The larger flakes were then removed from the suspension by centrifugation (6000 rpm, 15 min) and the residual supernatant with smaller size flakes was subsequently dried in vacuum and redispersed in methanol.

***The MXene flakes deposition on the grating surface**.* The suspension of MXene in methanol (0.3-7 mg/mL) was drop-deposited on the grating surface and spin-coated at 100-3000 rpm for 3 min. The deposition route was optimized for the reaching of a thin as possible homogeneous covering of the grating surface by flakes. After the optimization procedure (see main text for details), the 1.7 mg/mL MXene concentration and 1000 rmp were founded to be optimal.

Measurement Techniques

TEM images of MXene flakes were obtained with the help of a JEOL JEM-1010 transmission electron microscope with a SIS MegaView III digital camera. X-Ray diffraction measurements were carried out using the Empyrean, Malvern Panalytical diffractometer with Cu $K_{<\alpha>}$ radiation source in 2θ-θ diffraction mode, the Bragg-Brentano geometry. Raman spectra were measured using ProRaman-L spectrometer (Laser power 33 mW) with 785 nm excitation wavelength. Spectra were measured 30 times, each of them with 3 s accumulation time. Raman mapping was performed across a surface area of $1.3 \times 0.8\ mm^2$, having 70 × 40 points spaced by a gap of 0.025 mm. The peak force AFM measurements were performed using the Icon (Brucker) microscope. SEM-EDX photos and maps were obtained on Lyra3 GMU (Tescan, CR) microscope with an accelerating voltage of 2 kV.

The X-ray photoelectron spectroscopy was performed using an Omicron Nanotechnology ESCAProbeP spectrometer fitted with a monochromated Al K_{Alpha} X-ray source working at 1486.6 eV. Concentrations of elements were calculated in at.% using the manufacturer's sensitivity factors. UV-Vis absorbance spectra of the samples were measured using a Lambda 25 spectrometer (PerkinElmer, USA). Semiquantitative determination of Au and Ti concentrations in electrolyte solution was performed on ICP-MS/MS spectrometer (Agilent 8900) in He and O_2 mode. Two point calibration was prepared from Agilent PA tuning multielemental standard solutions.

Optimization of Au grating structure.

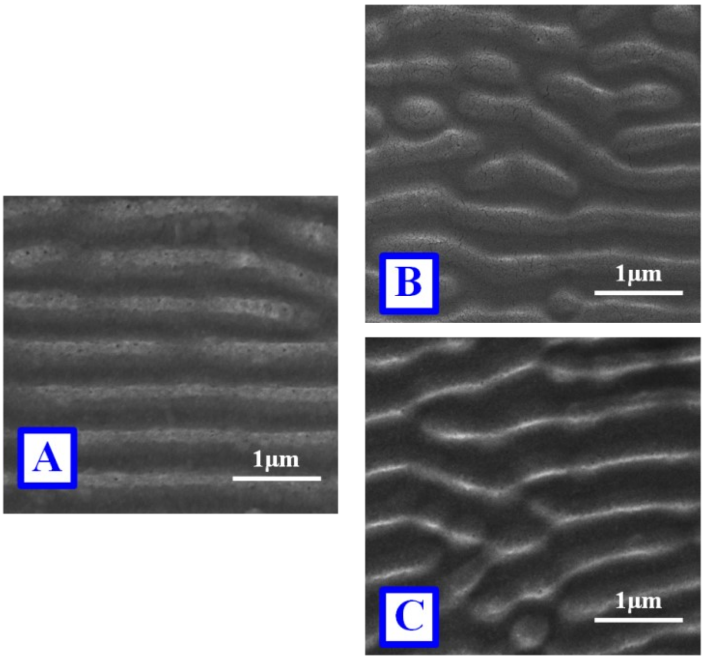

Fig. S1 SEM image of (A) – optimized Au grating;(B, C) – un-optimized Au grating (incorrectly tuned excimer laser mode: increased laser power or incorrect laser incident angle).

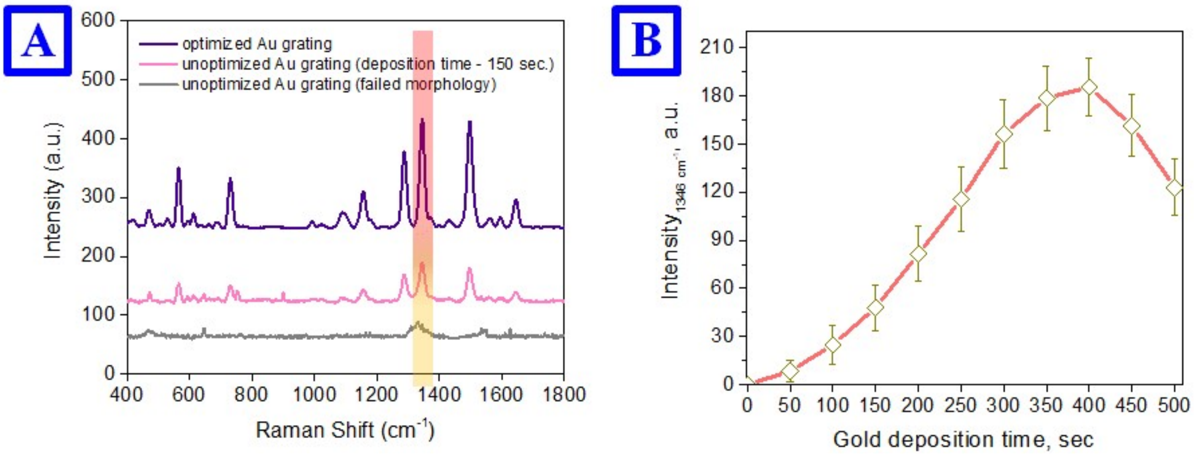

Fig. S2 (A) – Raman spectra of R6G on an un-optimized Au grating, optimized Au grating and on Au/ $Ti_3C_2T_x$ sample; (B) – Dependence of R6G intensity on different gold deposition times.

Fig. S1, Fig. S2 – description note.

Optimization of the grating structure was performed with the aim to reach the strongest SPP wave excitation, which is needed for the efficient triggering of the overlying MXene layer. The necessary conditions for SPP excitation are a high degree of grating periodicity and regularity. The optimal grating geometry was reached through the optimization of excimer laser pattering conditions. As an example, Fig. S1 gives the periodical grating structure (part A) and several "failed" structure morphologies corresponding to high laser power or incorrect incident angle. More detailed description of the grating preparation can be found in our previous works [S2, S3].

The next important parameter for efficient SPP excitation is the amount (thickness) of deposited metal. It was demonstrated previously e.g. in [S4], that there is some optimal range in metal thickness, which corresponds to a more strong SPP excitation. For experimental checking of SPP strength, common SERS measurements with a model analyte (R6G) were performed (Fig. S2). R6G molecules were deposited on Au grating surface with different metal thickness from 10^{-6}M solution using spin-coating and SERS measurements at 780 nm Raman excitation wavelength were performed. Since R6G does not intrinsically absorbs 780 nm wavelength and does not create a charge transfer complex with the gold surface, the intensity of its SERS response is strongly related to the local intensity of the plasmonic evanescent field. Dependency of the characteristic R6G band as a function of Au thickness (determined by deposition time) is presented in Fig. S2. From Fig. S2 the optimal thickness (i.e., deposition time) for more efficient SPP excitation is evident. In all further experiments, we used the Au gratings prepared under optimal laser pattering conditions and deposition of optimal Au amounts.

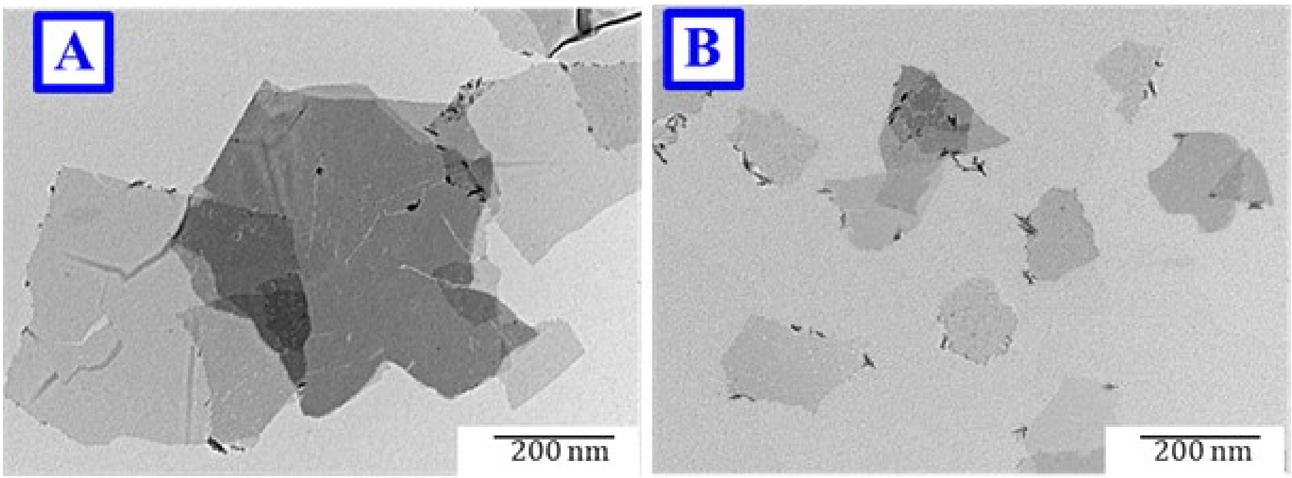

Fig. S3 TEM images of MXene flakes: (A) – after preparation by MILD method and (B) – after additional high power ultrasound treatment (*shredding*).

Fig. S3 – description note

The size of as-prepared MXene flakes was in the hundreds of nanometers range. Taking into account the rigidity of flakes, the homogeneous covering of gold grating morphological features (grating periodicity – 270 nm) with flakes penetration into valleys cannot be realized with such lateral flakes size. Thus, we applied the additional ultrasound treatment, with the aim to induce flakes shredding, but conserve their crystalline and chemical structure. We check several experimental routes, including the flakes treatment under medium power ultrasound for several hours, low power ultrasound treatment for several days, and high power ultrasound treatment for several minutes in various solvents. After experimental route optimization, the utilization of oxygen-free DMSO and application of several consecutive high-power ultrasound pulses during 15 min was found to be the optimal strategy to create flakes with smaller lateral size (Fig. S3).

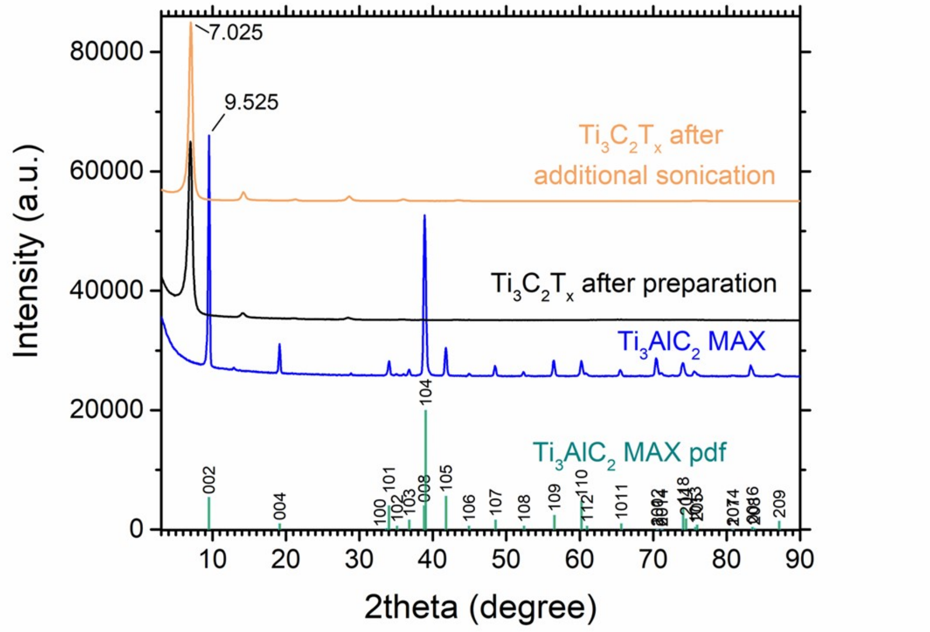

Fig. S4 XRD patterns of Ti_3AlC_2 MAX phase, MXene flakes prepared by MILD method and after additional sonication (absence of TiO_2 peaks). ICDD:00-052-0875 [S5].

Fig. S4 – description note

The diffraction pattern of Ti_3AlC_2 MAX phase corresponds to previous measurements [S5, S6] – the powder diffraction file from [S5] was used as a reference. Ti_3C_2 MXene prepared by MILD and sonication methods have shifted reflex due to delamination and surface modification of flakes. In particular, the key reflex (002) for Ti_3AlC_2 after delamination and surface termination by –F, –O, and –OH shifted from $2\theta = 9.525°$ to $2\theta = 7.025°$. In addition, most of the MAX phase peaks disappear during the delamination process. It should be also noted that the additional flake sonication does not lead to the changes of $Ti_3C_2T_x$ diffraction pattern and new peaks are not appears, indicating the conservation of flakes crystallinity and the absence of TiO_2 phase formation.

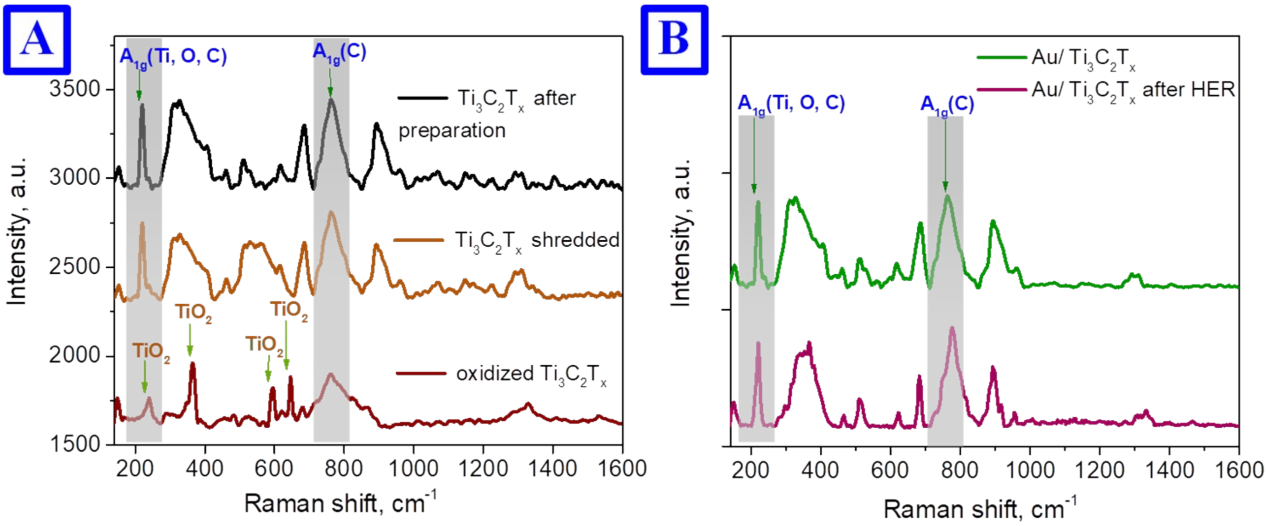

Fig. S5 A – Raman spectra of MXene flakes (after preparation by MILD method, after additional sonication, and control sample of oxidized MXene). B – SERS spectra of MXene flakes measured on $Ti_3C_2T_x$ /Au structure before and after its utilization in HER.

Fig. S5 – description note

The typical Raman spectrum of as-prepared flakes is shown in Fig. S5A. In this spectrum, there are two distinct sharp peaks, located near 220 cm^{-1} and 750 cm^{-1} and attributed to A_{1g} (Ti, O, C) and A_{1g}(C) vibration bands respectively. The ratio A_{1g}(C) / A_{1g}(Ti, O, C) is slightly above 1, which is typical for previously delaminated and stacked again in thin film structure MXene flakes [S7]. The additional high-power ultrasonication does not lead to the apparent changes of A_{1g}(C) and A_{1g}(Ti, O, C) peaks spectral positions and their relative ratio. The well-visible surface group region (230–470 cm^{-1}) conserves the overall shape during the flakes shredding, indicating the conservation of surface chemistry. Finally, the absence of titanium degradation is evident from the comparison of $Ti_3C_2T_x$ spectra after preparation and after additional sonication with the Raman spectrum of specially oxidized (by aging in oxygen-rich water) flakes. In the last case, the set of anatase and rutile characteristic peaks appears after oxidation (and the suspension colour changes from black to white). The absence of these peaks in the Raman spectra of as-prepared and shredded flakes clearly confirms the insignificant amount of TiO_2 phase in the used flakes.

We also performed the Raman measurements after the flakes deposition on Au grating and utilization of $Ti_3C_2T_x$/Au samples in the plasmon-triggered hydrogen evolution reaction (HER) reaction (10 hours light switching mode). Obtained results are presented in Fig. S5B. Since we used the 785 nm Raman excitation wavelength, which overlaps with both flakes and Au grating plasmon resonance, we did not observe any significant change in the characteristic A_{1g}(Ti, O, C) and A_{1g}(C) vibration bands intensities. Subsequent utilization of samples in plasmon-triggered HER conserves the intensities of these characteristic bands at the same initial level. Some increase of the broad band in 250–470 cm^{-1} spectra regions, responsible for the surface terminated groups. These changes can be attributed to the partial oxidation of MXene flakes, which is in agreement with the discussed below XPS results. However, despite the observed slight oxidation, the $Ti_3C_2T_x$/Au samples conserve their functionality in terms of HER light-sensitive catalyst (Figs. 3C and 4C).

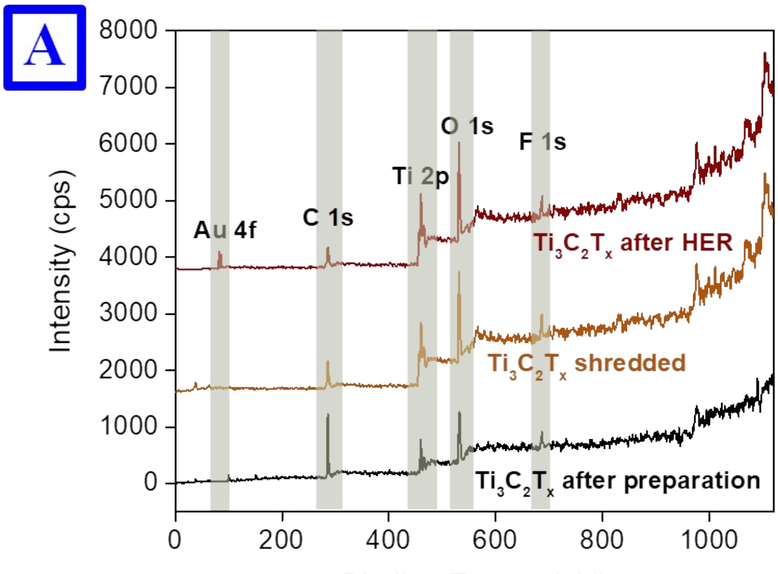

B

	Au 4f	C 1s	O 1s	Ti 2p	F 1s
$Ti_3C_2T_x$ after preparation	-	50.81	33.48	8.78	6.93
$Ti_3C_2T_x$ shredded	-	39.64	34.53	15.99	9.84
$Ti_3C_2T_x$ after HER catalytic performance	3.66	39.5	34.82	8.92	13.1

Fig. S6 (A) – XPS spectra of as-prepared (by MILD method) $Ti_3C_2T_x$ flakes, ultrasonically shredded flakes, and flakes after HER catalytic performance evaluation, (B) – elemental surface composition, calculated from XPS spectra for $Ti_3C_2T_x$ flakes, ultrasonically shredded flakes, and flakes after HER catalytic performance evaluation.

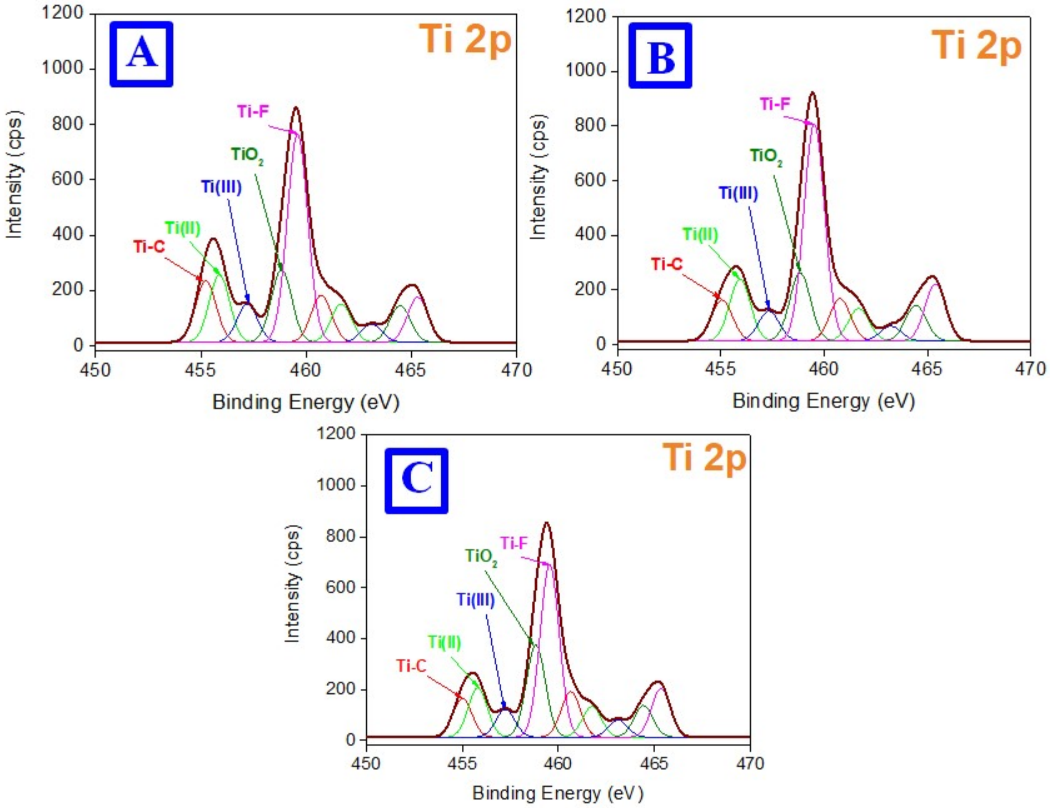

D

	S (TiO2)/S (Ti-C)	S (Ti(II) + Ti(III))/S (Ti-C)	S (Ti-F)/S (Ti-C)
$Ti_3C_2T_x$ after preparation	1.785	2.639	4.122
$Ti_3C_2T_x$ shredded	2.525	3.393	6.673
$Ti_3C_2T_x$ after HER	3.199	3.235	5.731

Fig. S7 XPS spectra of Ti 2p, O 1s, C 1s, F 1s regions of (A) – $Ti_3C_2T_x$ flakes after preparation by MILD method, (B) – $Ti_3C_2T_x$ flakes after additional sonication, (C) – $Ti_3C_2T_x$ flakes after utilization in HER, (D) – relative Ti deconvoluted peaks areas, calculated for as-prepared $Ti_3C_2T_x$ flakes by MILD method, ultrasonically shredded flakes, and flakes after HER catalytic performance testing.

Fig. S6, S7 – description notes

The chemical composition of $Ti_3C_2T_x$ flakes was investigated by XPS after MAX phase etching and delamination by MILD method, additional flakes shredding, and after utilization of MXene thin film as a HER catalyst under switched plasmon triggering (Fig. S6). Additionally, the deconvolution of Ti peaks allows us to analyse the oxidation states of Ti and the potential formation of TiO_2 at all stages of flakes preparation/utilization (Fig. S7). As is evident from XPS graph (Fig. S6), the Al was completely removed from the initial MAX phase. Additional flake shredding under optimized conditions doesn't lead to a significant increase of oxygen surface concentration, indicating the absence of significant Ti oxidation. In turn, the utilization of flakes in plasmon assisted HER during 10 hours led to only a slight shift of chemical composition, mainly in terms of relative Ti/O surface concentration.

Deconvolution of Ti XPS peaks further allows us to estimate the chemical changes of Ti during the preparation and utilization (Fig. S7). First, on the pristine flakes, the apparent peaks related to Ti-C, Ti(II), Ti(III), Ti-F, and TiO_2 are evident. Since the Ti-C peak can be used as an internal XPS standard for the estimation of $Ti_3C_2T_x$ surface termination, we used the comparison of its area with others peaks (Fig. S7 D) As is evident, the flakes shredding does not affect the (Ti(ii)+Ti(iii))/Ti-C, Ti-F/Ti-C, and TiO_2/Ti-C ratios. In turn, the subsequent utilization of flakes in plasmon-assisted HER led to a slight increase of TiO_2 / Ti-C ratio, an indication that some oxidation of titanium still occurs. However, the observed increase is not so significant and, in general, does not lead to apparent HER efficiency deterioration.

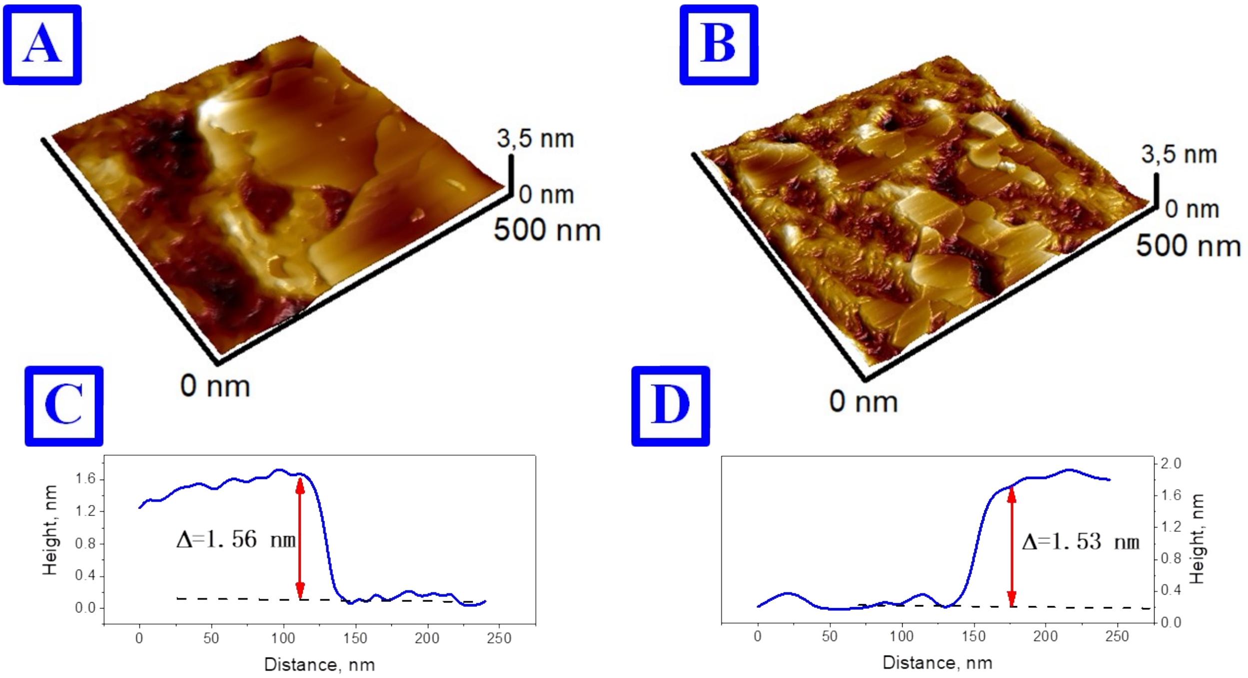

Fig. S8 A, B – AFM measured the morphology of as-prepared and shredded flakes deposited on a flat substrate, C, D – corresponding surface profiles, taken across the flake boundaries and related flakes thickness estimation.

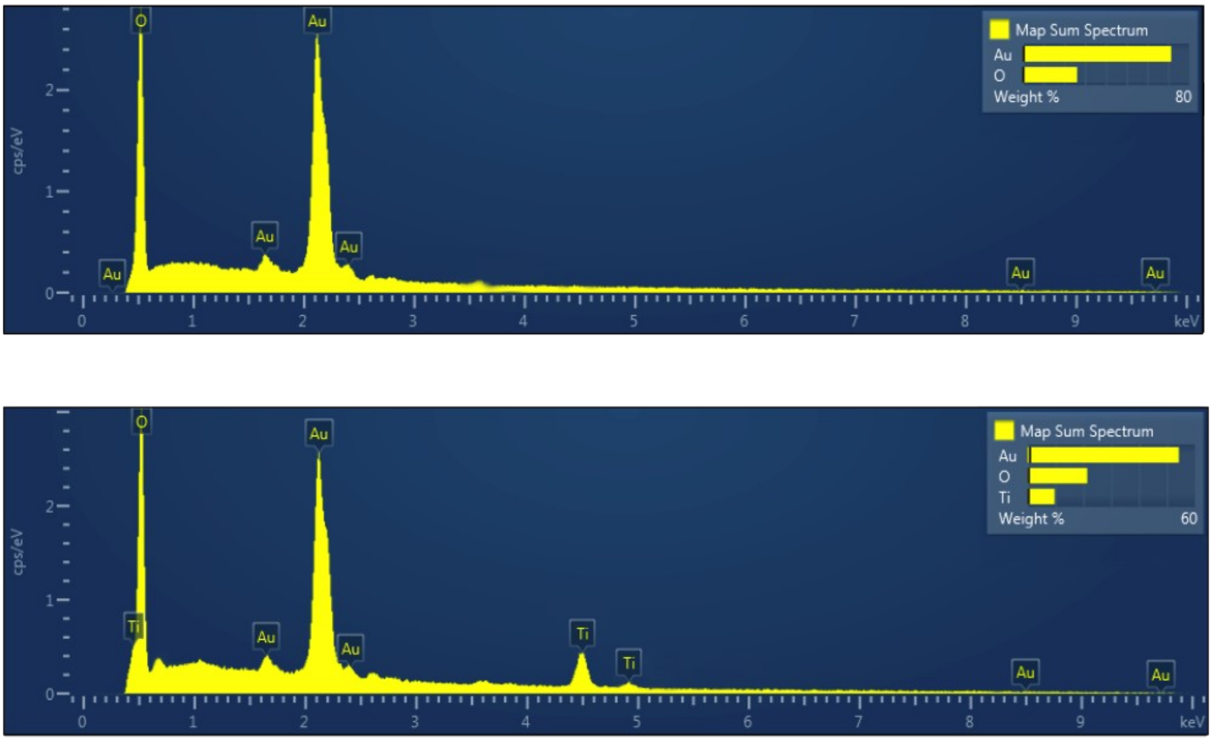

Fig. S9 Elemental analysis (EDX) of the pristine Au grating and Au grating with MXene layer (just Au and Ti characteristic peaks are highlighted), deposited at “optimal” conditions.

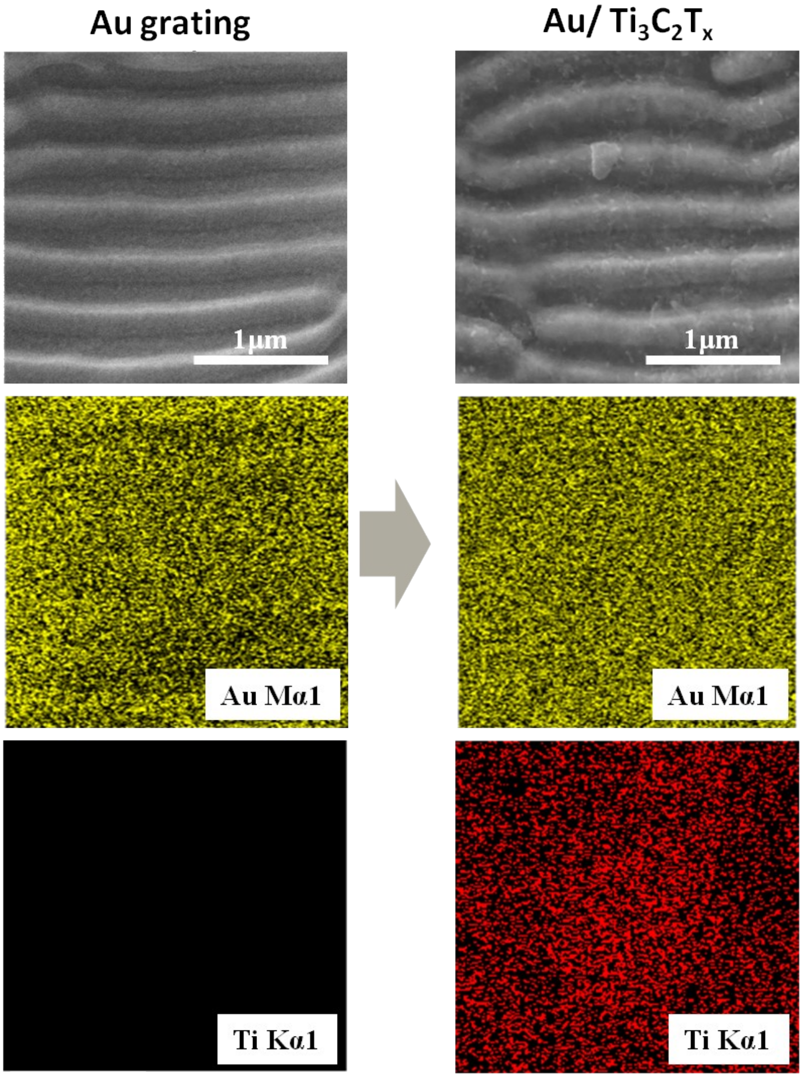

Fig. S10 SEM-EDX mapping (with higher magnification) of the pristine Au grating and Au grating with MXene layer, deposited at "optimal" conditions.

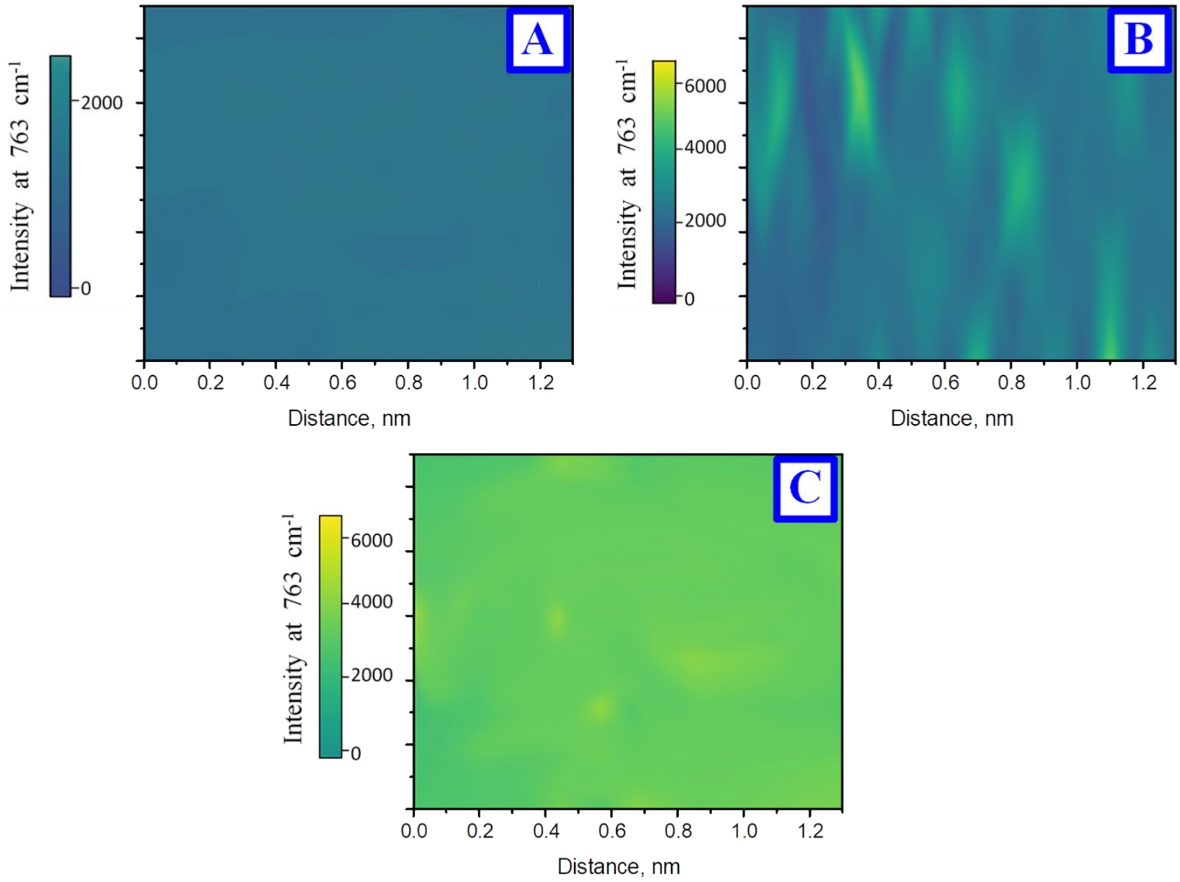

Fig. S11 Raman mapping of MXene distribution (intensity of 763 cm^{-1}, characteristic peak is used as a marker): (A) – pristine Au grating sample, (B) – Au grating with "nonhomogeneous" distribution of MXene flakes (see description note), and (C) – Au grating with optimized, "homogeneous" distribution of MXene flakes (see description note).

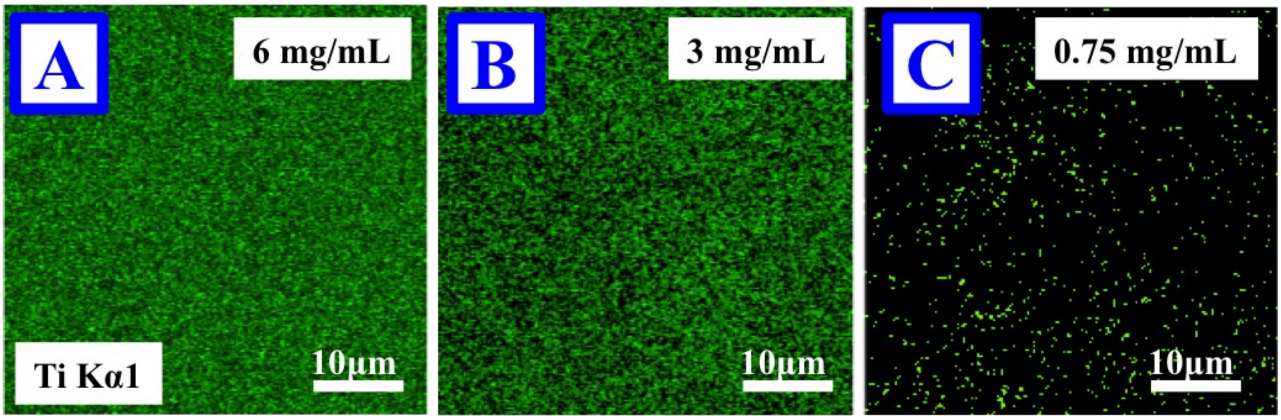

Fig. S12 EDX mapping of Ti distribution during the MXene deposition route optimization.

Fig. S9-S12 – description note

The optimization of MXene flakes distribution was performed using the solutions with different concentrations (0.5 – 7 mg/mL concentration range) of flakes suspension and the speed of spin-coating (100 – 3000 rmp). The main aim of the applied procedure was to reach as thin as possible MXene flake layer, a homogeneously coated grating surface.

The homogeneity of flakes distribution was checked using the SEM-EDX measurements and Raman mapping. The final and intermediate results of the optimization procedure are presented in Figs. S9-S12. In particular, it was founded that the application of lower spin-coating speed led to the apparent flake agglomeration during the deposition, and the formation of apparent island-like structures. The increase of spin-coating speed up to ca 1000 rpm allows to reach the more homogeneous covering of the grating surface (Fig. S11 C). In turn, the implementation of higher spin-coating speed results in worse covering, since most of the flakes were removed under centrifugal force (Fig. S11 B). Thus, we choose 1000 rmp for flakes deposition.

Additionally, the initial flakes concentration also affects the flakes distribution. In particular, the Fig S12 B shows the apparent homogeneous Ti distribution, reached at 1000 rpm from the 6 mg/ml suspension. However, twice dilution of suspension conserved the homogeneity of flakes distribution (Fig. S12 B). Further dilution of the suspension led to an apparently nonhomogeneous covering of the gold grating (Fig. S12 C).

Thus, after optimization of the deposition conditions of MXene flakes on the periodical gold grating surface, we chose the initial concentration to be 3 mg/ml and 1000 rpm spin-coating speed.

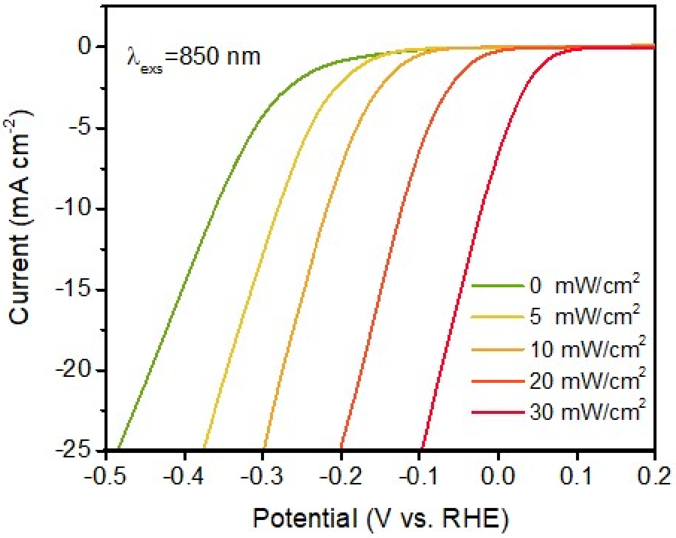

Fig. S13 (A) – LSV curves measured under different light powers of LED (850 nm); (B,C) – calculated values of Tafel slope for Au/ $Ti_3C_2T_x$ samples, measured under different light power (850 nm).

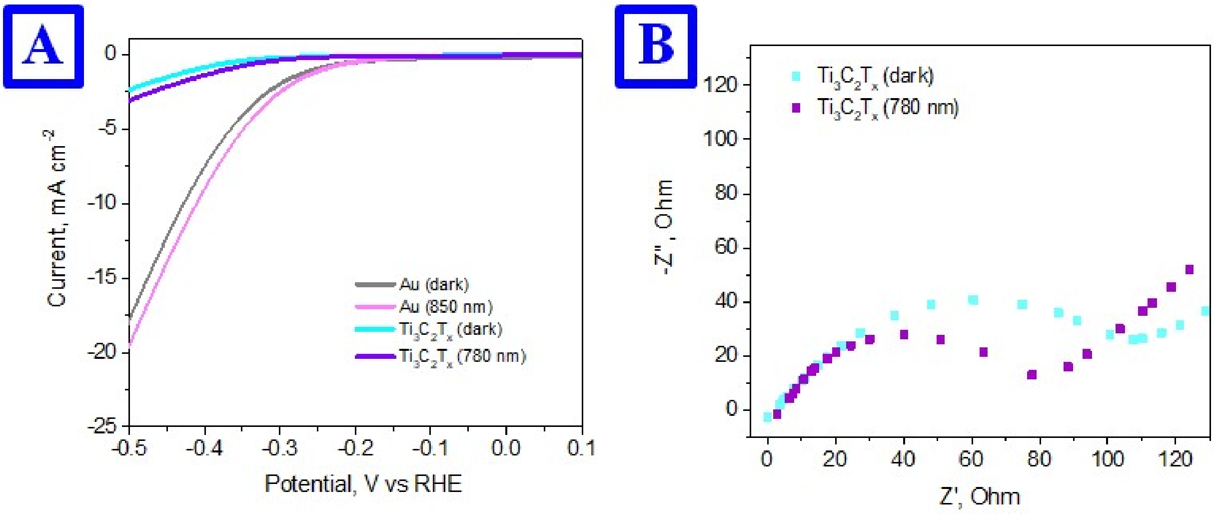

Fig. S14 (A) – linear sweep voltammetry curves of pristine Au grating and $Ti_3C_2T_x$ flakes (on non-plasmon (carbon) substrate), measured in the dark and under illumination with wavelength, corresponding to plasmon absorption band excitation; (B) – results of electrochemical impedance spectroscopy of $Ti_3C_2T_x$ flakes, performed in dark or under illumination with 780 nm LED.

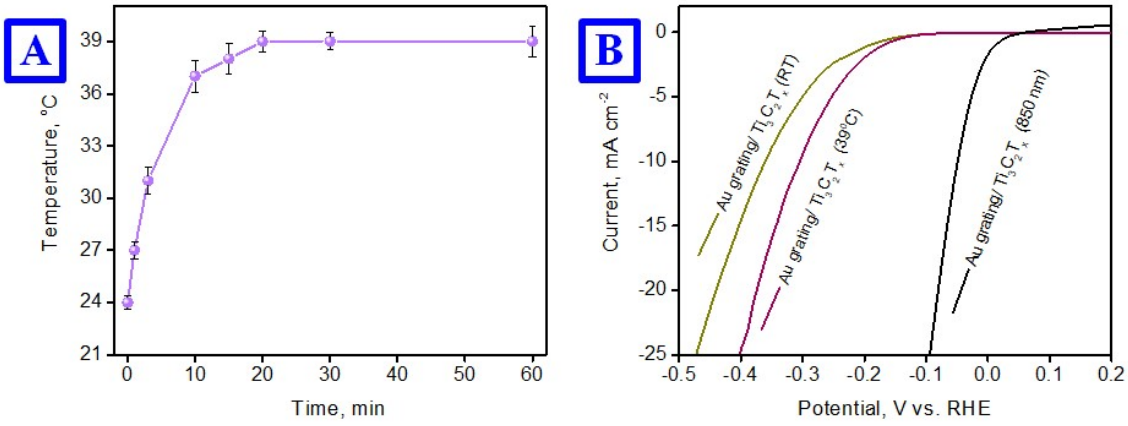

Fig. S15 (A) – temperature of the Au/ $Ti_3C_2T_x$ samples surface under illumination with 850 nm LED as a function of exposure time; (B) – LSV curves measured under RT and 39° C

Fig. S15 – description note

The experimental measurement of surface temperature was performed with an ultrathin thermocouple attached to a sample surface. Experiments were done in time-resolved regime with sample immersion in electrolyte solution and illumination with 850 nm LED. Obtained results indicate the gradual increase of surface temperature, which is saturated after ca 15 min of illumination. Such time interval is in good correlation with chronoamperometry, HER studies, and confirm our assumption regarding the contribution of plasmon heating to HER efficiency. It should be also noted that the apparent temperature increase was ca 15°C, but the real plasmon-assisted (nano) local heating can reach a significantly higher value.

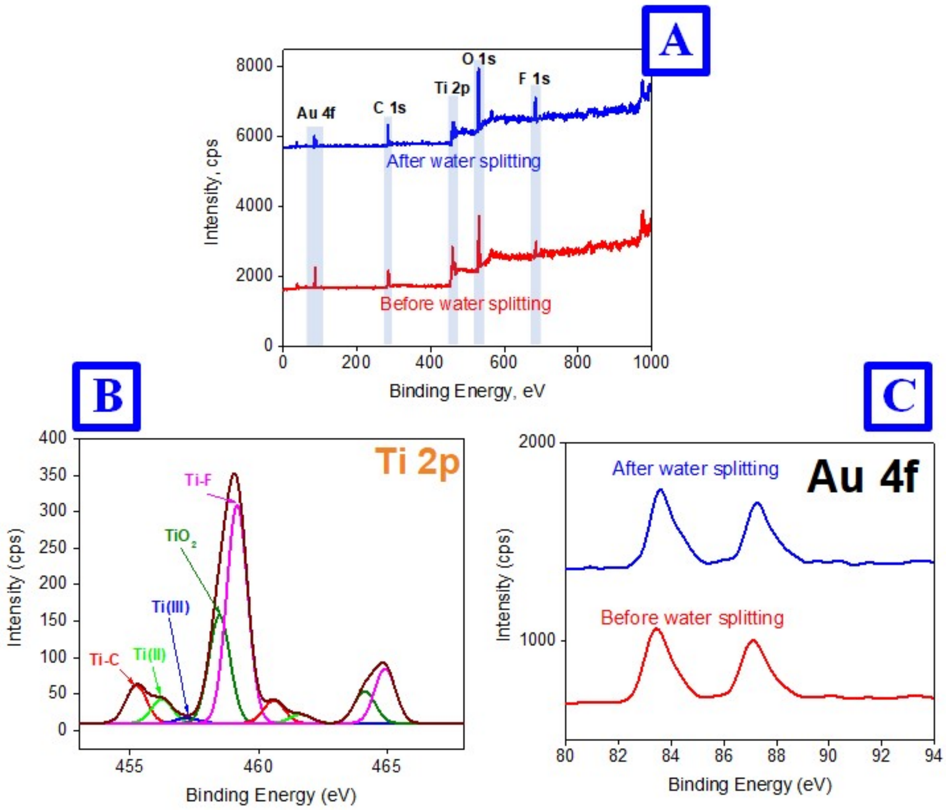

Fig. S16 XPS Evaluation of Au/$Ti_3C_2T_x$ surface composition after water splitting in two electrodes arrangement (0.01 M K_2CO_3 electrolyte, 10 h.).

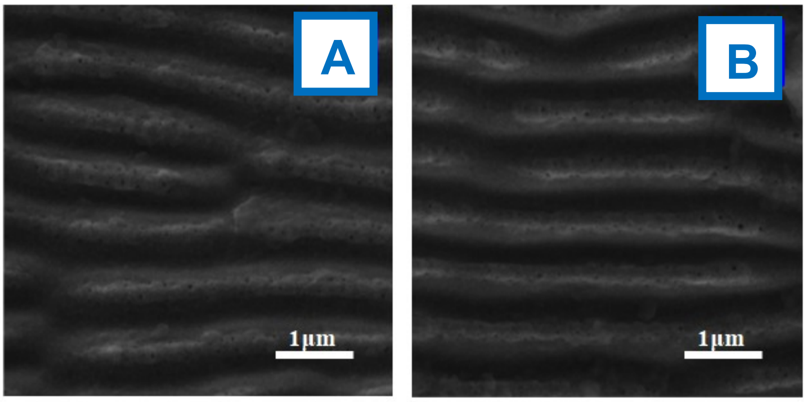

Fig. S17 SEM images of Au/$Ti_3C_2T_x$ samples surface, taken before (A) and after (B) hydrogen production in two electrodes system (10 h., 0.01 M K_2CO_3 water solution).

Fig. S16, Fig. S17 - description note

Additional examination of Au/$Ti_3C_2T_x$ (photo) electrode surface after sample involving in hydrogen production (two electrode system, 0.01 M K_2CO_3 electrolyte solution) was performed using the XPS (Fig. S16) and SEM (Fig. S17) methods. Results of XPS measurement indicate the conservation of the overall surface elemental composition (Fig. S16A). In turn, the comparison of Ti 2p detailed XPS scans (Fig. S7B vs Fig. S16B) confirms the absence of apparent Ti oxidation, which can be expected due to the higher stability of Ti (and $Ti_3C_2T_x$) under applied negative potential. Similar results were observed for Au, where the detailed XPS scan of Au 4f region indicates the conservation of relative characteristic peaks intensities and the peak shape, confirming the maintaining of the initial Au surface state. In turn, SEM measurements performed after Au/$Ti_3C_2T_x$ samples utilization in water for 10 h. (Fig. S17) show conservation of surface morphology, without the appearance of apparent defects. We also estimated the composition of the electrolyte solution after water splitting by ICP technique. In this case, we did not observe the characteristic signal from Ti and insignificant (0.8 ng/ml) concentration of Au ions, which confirms the negligible electrode degradation.

References

[S1] Y. Kalachyova, D. Mares, V. Jerabek, K. Zaruba, P. Ulbrich, L. Lapcak, V. Svorcik, O. and Lyutakov, *J. Phys. Chem. C,* 2016, **120(19)**, 10569-10577.

[S2] Y. Dong, S. Chertopalov, K. Maleski, B. Anasori, L. Hu, S. Bhattacharya, A. M. Rao, Y. Gogotsi, V. N. Mochalin, R. Podila, *Adv. Mater*., 2018, **30**, 1705714.

[S3] Y. Kalachyova, O. Lyutakov, P. Slepicka, R. Elashnikov and V. Svorcik, *Nanoscale Res. Lett.*, 2014, **9(1),** 1-10.

[S4] Y. Kalachyova, D. Mares, O. Lyutakov, M. Kostejn, L. Lapcak, and Svorcik, V. *J. Phys. Chem. C*, 2015, **119(17),** 9506-9512.

[S5] N. V. Tzenov and M. W. Barsoum, *J. Am. Ceram. Soc*., 2000, **83**, 825−832.

[S6] E. Wu, J. Wang, H. Zhang, Y. Zhou, K. Sun and Y. Xue, *Mater. Lett.,* 2005, **59(21)**, 2715-2719.

[S7] A. Sarycheva and Y. Gogotsi, *Chem. Mater.,* 2020, **32(8)**, 3480−3488.